Three-co-ordinated Transition-metal Compounds. Part II.[1] Electronic Spectra and Magnetism of Tris(bistrimethylsilylamido)derivatives of Scandium, Titanium, Vanadium, Chromium, and Iron

By **E. C. Alyea, D. C. Bradley,* R. G. Copperthwaite,** and **K. D. Sales,** Department of Chemistry, Queen Mary College, Mile End Road, London E1 4NS

The electronic spectra, magnetic susceptibilities, and preliminary e.s.r. data are reported for the trigonal compounds $M[N(SiMe_3)_2]_3$ where M = Sc, Ti, V, Cr, and Fe. The data are interpreted on the basis of crystal-field calculations for d^n systems in D_{3h} symmetry.

In the first paper in this series we described the preparation and characterization of the trigonal compounds $M[N(SiMe_3)_2]_3$ (M = Sc, Ti, V, Cr, and Fe). We now report the details of the electronic spectra and magnetic properties of these compounds which are of particular interest since they relate to d^n ($n = 0$, 1, 2, 3, and 5) electronic configurations in a low symmetry (D_{3h}) ligand field.

Although we regard these compounds as being substantially covalent in character it has been found useful to discuss the assignment of electronic transitions in terms of crystal-field calculations for the splitting of d orbital-energy levels in a trigonal planar (D_{3h}) field. The relevant details of these calculations are given in the Appendix.

$Sc[N(SiMe_3)_2]_3$.—Since this compound contains a d^0 metal ion the two bands observed in the u.v. region (Table 1) must be due to charge-transfer and/or ligand–ligand transitions and this has been borne in mind in interpreting the spectra of the following compounds.

TABLE 1

Electronic spectra of $M[N(SiMe_3)_2]_3$ compounds

M in $M[N(SiMe_3)_2]_3$	'd–d' Transitions [a]	Other electronic transitions [b]
Sc (d^0)	—	31·2 (*ca.* 500); 40·8 (*ca.* 1500)
Ti (d^1)	4·8 (10); $^2A_1' \longrightarrow {}^2E''$	28·6 (500)
	17·4 (122); $^2A_1' \longrightarrow {}^2E'$	
V (d^2)	12·0 (60); $^3E'' \longrightarrow {}^3E'$	24·7 (480); 28·1 (450)
	15·9 (150); $^3E'' \longrightarrow (^3A_1'', {}^3A_2'')$	
	19·2 (268); $^3E'' \longrightarrow {}^3E''$	
Cr (d^3)	11·8 (100); $^4A_2' \longrightarrow (^4A_1'', {}^4A_2'')$	25·3 (3700); 31·4 (3700)
	14·8 (540); $^4A_2' \longrightarrow {}^4E'$	33·6 (2800)
Fe (d^5)	16·1 (400); $^6A_1' \longrightarrow (^4A_1'', {}^4A_2'')$	25·3 (1500); 29·7 (1500)
	20·0 (450); $^6A_1' \longrightarrow {}^4E'$	

[a] Band maxima in 10^3 cm^{-1}; molar extinction coefficients in parentheses. [b] Probably charge-transfer and ligand-ligand transitions.

$Ti[N(SiMe_3)_2]_3$.—This bright blue compound has bands in the near i.r., visible, and u.v. regions (Table 1) and it is clear that the weak low-energy bands are due to d–d transitions. In D_{3h} symmetry the one-electron d orbitals transform as: $a_1'(d_{z^2})$; $e'(d_{xy},d_{x^2-y^2})$; $e''(d_{xz},d_{yz})$; hence only two d–d transitions are predicted. The two crystal-field parameters Ds and Dt are used to define the d orbital energies (adopting Wood's convention [2]) as follows: $a_1' = 2Ds + 6Dt$; $e' = -2Ds + Dt$; $e'' = Ds - 4Dt$.

The e.s.r. signal (g *ca.* 2) given by the compound in solution at room temperature and the magnetic moment close to the spin-only value for d^1 and independent of temperature (Table 3) require an orbital singlet ground state without low-lying excited states. Therefore the ground state must be $^2A_1'$ and the assignment of the bands at 4800 and 17,400 cm^{-1} corresponds to $Ds = -4286$ and $Dt = -51$ cm^{-1}. Support for these assignments is also given by the much lower intensity of the 4800 cm^{-1} band because the $^2A_1' \rightarrow {}^2E''$ transition is symmetry forbidden whereas $^2A_1' \rightarrow {}^2E'$ is symmetry allowed.

TABLE 2

Splitting of free-ion terms in D_{3h} field

Free ion	Terms in D_{3h}
^2D (Ti^{3+})	$^2A_1' + {}^2E' + {}^2E''$
^3F (V^{3+})	$^3A_2' + (^3A_1'', {}^3A_2'') + {}^3E' + {}^3E''$
^3P	$^3A_2' + {}^3E''$
^4F (Cr^{3+})	$^4A_2' + (^4A_1'', {}^4A_2'') + {}^4E' + {}^4E''$
^4P	$^4A_2' + {}^4E''$
^6S (Fe^{3+})	$^6A_1'$
^4G	$^4A_1' + (^4A_1'', {}^4A_2'') + {}^4E'(2) + {}^4E''$
^4P	$^4A_2' + {}^4E''$
^4D	$^4A_1' + {}^4E' + {}^4E''$
^4F	$^4A_2' + (^4A_1'', {}^4A_2'') + {}^4E'' + {}^4E'$

For the trigonal TiN_3 group, with the z-axis represented by the three-fold rotation axis, the electron density for σ-bonding should be concentrated in the x,y-plane thus raising the energy of the $d_{xy},d_{x^2-y^2}(e')$ orbitals in accordance with our assignment of energy levels: $e' > e'' > a_1'$. With one unpaired electron in the d_{z^2} orbital the system gains 8880 cm^{-1} in crystal-field stabilization energy.

We note that the observed g-value anisotropy (Table 3) is in accordance with the $^2A_1'$ ground state for an axially symmetric system. The detailed interpretation of this and the other e.s.r. spectra recorded in Table 3 will be given in Part III.

The g_0-value for the titanium compound corresponds to $\mu_{eff} \sim 1{\cdot}65$ B.M. whereas the magnetic susceptibility data (Table 8) plotted as $(\chi_M')^{-1}$ *vs.* T fit a Curie–Weiss equation with $\theta = -15°$ and $\mu = 1{\cdot}73$. However, the

[1] Part I, E. C. Alyea, D. C. Bradley, and R. G. Copperthwaite, *J.C.S. Dalton*, 1972, 1580.
[2] J. S. Wood, *Inorg. Chem.*, 1968, **7**, 852.

low-lying excited state ($^2E''$) contributes to the susceptibility by the second-order Zeeman effect giving rise to a T.I.P. of $4N\beta^2/\Delta E$, which with $\Delta E = 4800$ cm^{-1} corresponds to 217×10^{-6} c.g.s. units. The corrected susceptibility (χ_M'') now fits a Curie law, with an average value of $\mu_{eff} = 1{\cdot}62 \pm 0{\cdot}035$ B.M. in good agreement with that calculated from the g_0-value.

V[N(SiMe$_2$)$_2$]$_3$.—The absorption bands for this compound are given in Table 1. The low-energy bands (12,000 and 15,900 cm^{-1}) of weak intensity are assigned to d–d transitions whilst the intense high-energy band (28,100 cm^{-1}) is clearly due to a charge-transfer or ligand–ligand transition. The strong band at 24,700 cm^{-1}, by comparison with the data for the other compounds, is considered not to be due to a d–d transition whereas the weaker band at 19,200 cm^{-1} seems more likely to be so.

The splitting of the free-ion terms ^3F and ^3P for the V^{3+} ion (d^2) in a crystal field of D_{3h} symmetry are given in Table 2. To calculate the energies of these states we need a value for the Racah interelectron repulsion parameter B in addition to Ds and Dt; the free-ion value of 860 cm^{-1} was used for the following calculations. Calculations on the basis of either an orbital singlet or a $^3E'$ ground state failed to fit the observed d–d transitions but with $^3E''$ as the ground state a reasonable fit was given with $Ds = -5600$; $Dt = +100$ cm^{-1}; $Dt/Ds = -0{\cdot}0179$. Figure 1 shows the crystal-field diagram

TABLE 3

Magnetic properties of M[N(SiMe$_3$)$_2$]$_3$ compounds

M in M[N(SiMe$_3$)$_2$]$_3$	Ground state	μ_{eff}^T [a] 298 K	98 K	θ/°	g-Values [b] g_0	$g_\parallel$	$g_\perp$
Ti	$^2A_1'$	1·62 [c]	1·62 [c]	0	1·911	1·993	1·869
V	$^3E''$	(2·38) [d]			N.s.[e]	N.s.	N.s.
Cr	$^4A_2'$	3·74	3·70 [f]	−4	N.s.	2	4
Fe	$^6A_1'$	5·94	5·94	−10	N.s.	2	6

[a] From $\mu_{eff}^T = 2{\cdot}84\,[\chi_M'(T - \theta)]^{\frac{1}{2}}$, where χ_M' = molar susceptibility after correction for diamagnetic contributions. [b] g_0 Is the isotropic value obtained from solution spectrum at 298 K; $g_\parallel$ and $g_\perp$ obtained from powder or low temperature frozen solution spectra; for Cr^{3+} (d^3) and Fe^{3+} (d^5) effective g values are quoted. [c] Average value over the whole temp. range (see Table 8). [d] From a measurement at 298 K assuming Curie law behaviour. [e] N.s. = No signal observed. [f] This value is for $T = 123$ K.

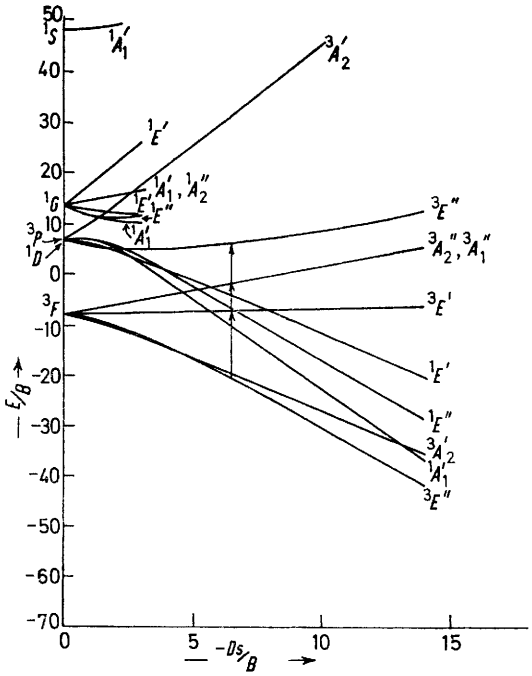

FIGURE 1 Crystal-field diagram for V[N(SiMe$_3$)$_2$]$_3$

calculated for this ratio of $Dt:Ds$. The calculated energies for the expected transitions are given in Table 4. The lowest-energy transition ($^3E'' \rightarrow {}^3A_2'$) was not detected because it is in the far-i.r. region; the energy of 800 cm^{-1} for this transition would lead to a 2% population of the $^3A_2'$ state at room temperature. However, on the basis of the detailed calculations we believe this value to be the lower limit and the population of $^3A_2'$ to be negligible. The highest-energy transition [$^3E'' \rightarrow {}^3A_2'(P)$] would be obscured by the charge-transfer or ligand–ligand band in the u.v. region. Somewhat better agreement between observed and calculated energies could be obtained by lowering B to 80% of its free-ion value, when we calculate: $^3E'' \rightarrow {}^3E'$ at 11,900 cm^{-1}; $^3E'' \rightarrow ({}^3A_1'', {}^3A_2'')$ at 15,700 cm^{-1}; and $^3E'' \rightarrow {}^3E''$ at 21,100 cm^{-1}, for $Ds = -5300$ cm^{-1} and $Dt = 150$ cm^{-1}. The values of Ds and Dt given in Table 7 correspond to a crystal-field stabilization energy of 15,464 cm^{-1} for this d^2 trigonal system. It was not possible to determine μ_{eff} accurately by experiment but the value obtained at room temperature is reasonably near to the spin-only value for a d^2 ion.

TABLE 4

Assignment of d–d transitions for V[N(SiMe$_3$)$_2$]$_3$

Transition		Energy of transition (cm^{-1}) Calc.	Obs.	ε_M
$^3E'' \rightarrow {}^3A_2'$ (F)	Forbidden	800		
$\rightarrow {}^3E'$	Allowed	11,500	12,000	60
$\rightarrow {}^3A_1'', {}^3A_2''$	Forbidden	16,100	15,900	150
$\rightarrow {}^3E''$	Allowed	23,200	19,200	268
$\rightarrow {}^3A_2'$ (P)	Forbidden	44,400		

Cr[N(SiMe$_3$)$_2$]$_3$.—The absorption bands for this compound (see Table 1) are readily classified in terms of d–d

and charge-transfer or ligand–ligand transitions. Although the band at 14,800 cm^{-1} has a relatively large molar extinction coefficient, nevertheless, because of its position, we propose that it is due to a *d–d* transition.

TABLE 5

Assignment of *d–d* transitions for $Cr[N(SiMe_3)_2]_3$

Transition		Energy of transition (cm^{-1}) Calc.	Obs.	ε_M
$^4A_2' \rightarrow {}^4A_1'', {}^4A_2''$	Allowed	11,800	11,800	100
$\rightarrow {}^4E'$	Allowed	14,800	14,800	540
$\rightarrow {}^4E''(F)$	Forbidden	16,100		
$\rightarrow {}^4A_2'(P)$	Forbidden	39,100		
$\rightarrow {}^4E''(P)$	Forbidden	49,100		

For the Cr^{3+} ion (d^3) the free-ion terms ^4F and ^4P split into the states given in Table 2. The presence of an e.s.r. absorption at room temperature for the solid and the temperature-independent magnetic moment close to the spin-only value for three unpaired electrons is consistent with an orbital singlet ground-state. We assume that $^4A'_2$ is the ground state when the assignments shown in Table 5 may be obtained with the free-ion value of B (1030 cm^{-1}) and $Ds = -7045$ cm^{-1}; $Dt = 404$ cm^{-1}; $Dt/Ds = -0{\cdot}0573$. A crystal-field diagram for this ratio of Dt to Ds is shown in Figure 2. The assignment is not unambiguous because only two *d–d* transitions are observed experimentally. It seems probable that the symmetry-forbidden transition $^4A_2' \rightarrow {}^4E''(F)$ is so close in energy to the allowed

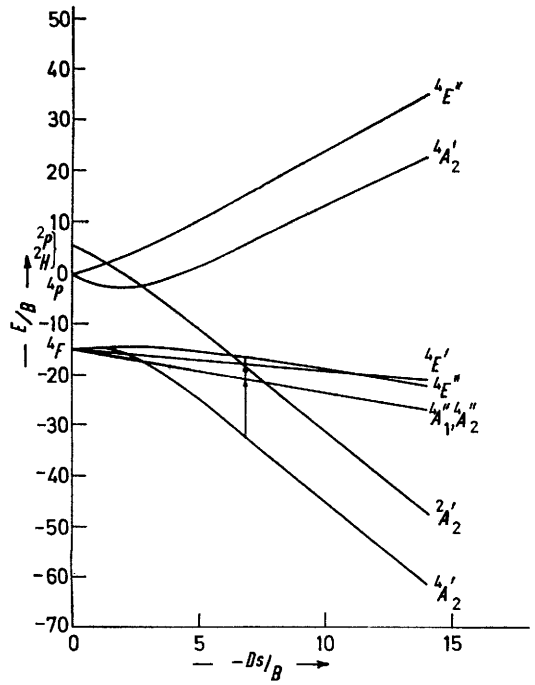

FIGURE 2 Crystal-field diagram for $Cr[N(SiMe_3)_2]_3$

transition $^4A_2' \rightarrow {}^4E'$ that it would be lost in such a broad band. Similarly the two symmetry-forbidden transitions in the u.v. region (calc. 39,100 and 49,100 cm^{-1}) would be masked by the intense charge-transfer transition at 31,400 cm^{-1}. Using the above values of Ds and Dt leads to a value of 29,000 cm^{-1} for the crystal-field stabilization energy for the d^3 ion in this trigonal compound.

$Fe[N(SiMe_3)_2]_3$.—With a half-filled *d*-shell the Fe^{3+} (d^5) ion has a ^6S term which cannot be split by a crystal

TABLE 6

Assignment of *d–d* transitions for $Fe[N(SiMe_3)_2]_3$

Transition		Energy of transition (cm^{-1}) Calc.	Obs.	ε_M
$^6A_1' \longrightarrow {}^4A_1'', {}^4A_2''$	Allowed	16,100	16,100	400
$\longrightarrow {}^4E''(G)$	Forbidden	16,600		
$\longrightarrow {}^4E'$	Allowed	20,000	20,000	450
$\longrightarrow {}^4A_1'(G)$	Forbidden	29,600		
$\longrightarrow {}^4E''(P)$	Forbidden	30,700		
$\longrightarrow {}^4A_2'(P)$	Forbidden	34,200		

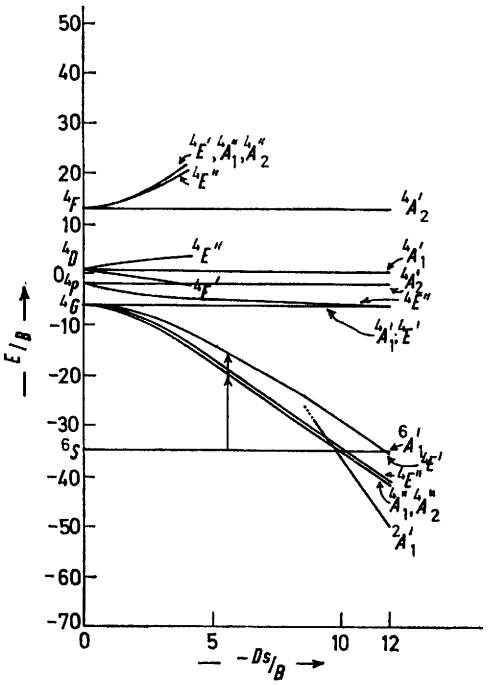

FIGURE 3 Crystal-field diagram for $Fe[N(SiMe_3)_2]_3$

field but low-lying quartet terms (^4G, ^4P, ^4D, ^4F) are present and the states arising from these in D_{3h} symmetry are given in Table 2. The magnetic and e.s.r. data (Table 3) define the ground state as $^6A_1'$ and all *d–d* transitions must be spin-forbidden. Even the weakest bands in the electronic spectrum (Table 1) seem rather intense for spin-forbidden transitions but the bands at 16,100 and 20,000 cm^{-1} are considered to be too low in energy for charge-transfer transitions and are therefore taken as *d–d* transitions. Using the Racah parameters for Cr^{3+} ($B = 1030$; $C = 3850$ cm^{-1}), since values for Fe^{3+} are not available, the assignments of Table 6 were made with $Ds = -5800$; $Dt = 770$ cm^{-1}; $Dt/Ds = -0{\cdot}1323$. The crystal-field diagram for this ratio is shown in Figure 3.

The failure to observe a band for $^6A_1' \rightarrow {}^4E''(G)$ is not surprising since the energy of this symmetry-forbidden transition is very close to the allowed band at 16,100 cm^{-1}. Similarly u.v. bands at energies greater than 25,000 cm^{-1} would be masked by the intense charge-transfer bands (see Table 1). For the high spin half-filled shell there is, of course, no crystal-field stabilization energy.

DISCUSSION

A summary of the results is presented in Table 7. The simple electrostatic model, assuming hydrogenic d orbitals and an effective nuclear charge Ze, predicts the ratio Dt/Ds to be negative. Whilst we would not necessarily expect agreement with this ratio obtained from the electronic spectra, it is interesting to note that, except for Ti^{3+}, the sign is in fact negative. Moreover, the Dt value for Ti^{3+} is only slightly negative and a shift, within the observed line width, in the position of the band at 4800 cm^{-1} (Table 1) would be sufficient to make Dt slightly positive. Furthermore, the calculated ratios for $Z = 3$ and 4 are −0·39 and −0·22 respectively, which are of a similar order to those of Table 7. It is clear from the data in Table 7 that considerable splitting of the d orbitals has occurred and that (except for Fe^{3+}) substantial amounts of crystal-field stabilization energy are present, increasing in the order $Ti^{3+} < V^{3+} < Cr^{3+}$. This may well contribute to a contraction of the M–N bond lengths as revealed by X-ray structural analysis.[3] From the energy-level diagram (Figure 4) it can be seen that in most cases (Ti^{3+}, V^{3+}, Cr^{3+}) the d_{z^2} orbital is lowest in energy but in Fe^{3+} the d_{xz},d_{yz} degenerate orbitals are lowest. In all cases the d_{xz},d_{yz} orbitals are stabilized by the crystal-field whereas the d_{xy}, $d_{x^2-y^2}$ orbitals are destabilised, as would be expected since the crystal field is mainly generated in the x,y plane.

Although attempts to prepare the Mn^{III}, d^4 complex have so far failed [1] there seems to be no reason from a crystal-field viewpoint why such a compound should not be stable and similar comments apply to the Co^{III}, d^6 compound. It is significant that the ferric compound is high spin, indicating a pairing energy > 20,000 cm^{-1}, and reference to Figure 3 shows that spin pairing would require $|Ds| > 10{,}200$ cm^{-1}. The interesting Mössbauer spectrum of the iron compound has been reported [4] and it is noteworthy that the sign of the principal component of the electric-field gradient tensor is positive corresponding to more negative charge in the x,y plane compared with the z-direction.

TABLE 7

Crystal-field parameters for $M[N(SiMe_3)_2]_3$

	Ti^{3+}, d^1	V^{3+}, d^2	Cr^{3+}, d^3	Fe^{3+}, d^5
Ds	−4·286	−5·600	−7·045	−5·800
Dt	−0·051	0·100	0·404	0·770
Dt/Ds	+0·012	−0·018	−0·057	−0·132
$\varepsilon(a_1')$	−8·880	−10·600	−11·666	−6·980
$\varepsilon(e'')$	−4·080	−6·000	−8·661	−8·880
$\varepsilon(e')$	+8·521	+11·300	+14·494	+12·370
C.F.S.E.	−8·880	−16·600	−28·988	0

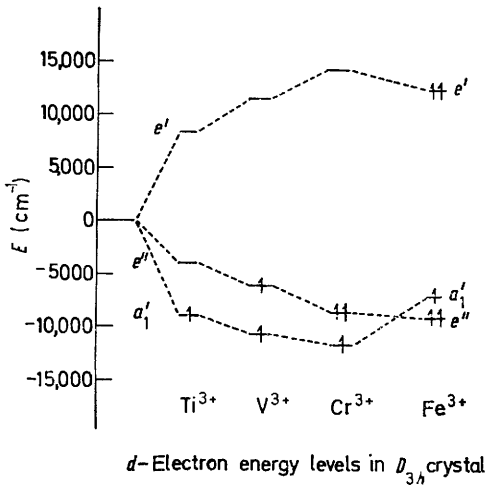

FIGURE 4 Energy levels for the d-orbitals in $M[N(SiMe_3)_2]_3$

The following additional experimental facts lead us to consider a qualitative molecular orbital diagram. Mass-spectral studies,[1] which revealed parent molecular ions and important fragment ions, indicate the considerable stability of the MN_3 framework. Another important feature concerns the geometry of these compounds.[3] The $MNSi_2$ groups are planar implying the possibility of π-bonding but the $MNSi_2$ planes make dihedral angles (θ) of *ca.* 50° with the MN_3 trigonal plane making the molecular point group D_3. Models indicate that the completely planar conformation (θ = 0) is prevented by interligand repulsions but that the alternative D_{3h} conformation (θ = 90) is feasible.

A qualitative molecular orbital diagram for the σ-bonding in an MN_3 moiety possessing D_{3h} symmetry is shown in Figure 5. It is comparatively easy to position the three occupied bonding MO's $[(a_1')_1 + (e')_1]$ and the three unoccupied antibonding MO's $[(a_1')_3 + (e')_3]$. However, apart from the non-bonding metal d–(e'') and p–(a_2'') orbitals the positions of the intermediate levels are not self-evident because they involve complicated mixtures of metal and ligand orbitals. Nevertheless it is obvious that the order of the $(e')_2$, (e''), and $(a_1')_2$ levels could easily be made to correspond to those of the d-orbitals e', e'', and a_1' in the crystal-field diagram (Figure 4).

If ligand → metal π-bonding is considered then the D_{3h} all-planar conformation (θ = 0) is favoured relative to the less sterically hindered D_{3h} conformation (θ = 90).

[3] D. C. Bradley, M. B. Hursthouse, and P. F. Rodesiler, *Chem. Comm.*, 1969, 14; M. B. Hursthouse and P. F. Rodesiler, *J.C.S. Dalton*, 1972, 2100; C. E. Heath and M. B. Hursthouse, to be published.

[4] E. C. Alyea, D. C. Bradley, R. G. Copperthwaite, K. D. Sales, B. W. Fitzsimmons, and C. E. Johnson, *Chem. Comm.*, 1970, 1715.

This is because the only orbitals on the nitrogen atoms of the ligands available for π-bonding are the $2p_z$ which in the first case generate the representations $a_2'' + e''$, which can interact with the metal p_z and d_{xz}, d_{yz}. Thus, with σ-bonding, all of the metal orbitals are brought into play. However, in the second case the $2p_z$ orbitals transform as $a_2' + e'$ which cannot interact with the metal orbitals because there is no metal orbital with a_2' symmetry and the e' representation is already concerned with σ-bonding. Thus it could be argued that the ligands adopt the intermediate D_3 conformation ($\theta = 50°$) as a compromise between steric interactions and the desire of the metal to involve all of its valence orbitals in bonding. The nature of the π-bonding would be expected to depend on the d^n configuration of the metal M^{3+} ion. For $Sc^{3+}(d^0)$ and $Ti^{3+}(d^1)$ the metal e'' orbitals are vacant and should act as acceptor orbitals (ligand → metal π-donation) thus raising the energy of empty, antibonding e'' (π) orbitals, increasing the M–N bond strength, and decreasing the NSi_2 π-bonding in the ligand. For $V^{3+}(d^2)$, $Cr^{3+}(d^3)$, and $Fe^{3+}(d^5)$ the antibonding e'' (π) orbitals are singly occupied diminishing the degree of π-bonding and lowering the energy of the

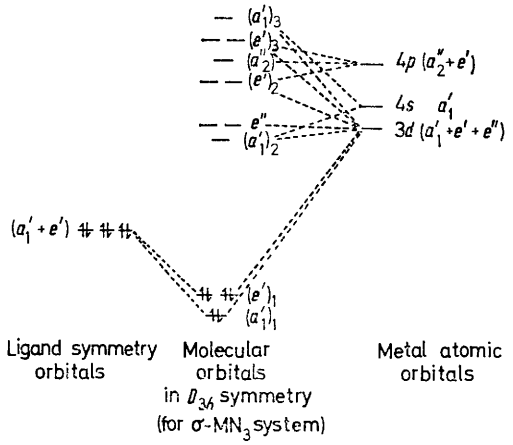

FIGURE 5 Qualitative molecular orbital diagram for MN_3 σ-bonding

antibonding e'' (π) orbitals; compare the stabilisation of the e'' orbitals shown by crystal-field theory (Figure 4).

EXPERIMENTAL

The compounds were prepared as described in Part I.[1]

Electronic Spectra.—A Beckmann DK-2A instrument was used over the spectral range 160—2500 nm with special attention to the region (5000—20,000 cm^{-1}) where *d–d* bands were expected. To avoid contamination of these very air-sensitive compounds an all-glass vacuum line was used to prepare solutions (cyclo-hexane) quantitatively for use in sealed silica cells (2·0 cm path-length). The results are given in Table 1.

E.s.r. Spectra.—A Decca X3 spectrometer operating at *X*-band frequency (9270·242 MHz) with a Newport M4X (11 in) magnet and Decca MW 235 variable-temperature (−175 to +100°) cavity insert was used. Some results are given in Table 3; full details of the e.s.r. spectroscopy will be given in a following publication dealing with oriented single-crystal and *Q*-band experiments.

Magnetic Susceptibility Determination.—A Newport variable-temperature Gouy balance was used over the range −175 to +100°. All measurements were carried out at three values of the field strength (3785, 5750, and 6675 G). Calibrations were doubly checked using mercury tetrathiocyanatocobaltate(II) ($\chi_g = 16{\cdot}44 \times 10^{-6}$ c.g.s. at 298 K) and trisethylenediaminenickel(II) thiosulphate ($\chi_g = 10{\cdot}83 \times 10^{-6}$ c.g.s. at 298 K) as standards. Attempts to grind samples and pack the Gouy tube even in a very good ' dry-box ' gave unreliable results using $Fe[N(SiMe_3)_2]_3$ and a special technique was developed to avoid the thermal decomposition incurred by grinding. An all-glass vacuum line was used which allowed a solution to be prepared (as for the electronic absorption spectra) out of contact with air. The solution was then ' freeze-dried ' *in vacuo* giving a fine powdery solid which was transferred to the Gouy tube

TABLE 8

Magnetic susceptibility data for $Ti[N(SiMe_3)_2]_3$

T (K)	$(10^6\chi_M'')$ [a]	(μ_{eff}^T) [b]
298	1056	1·59
273	1196	1·62
223	1487	$1{\cdot}63_5$
173	1775	1·57
123	2594	1·60
98	3546	1·67

[a] $\chi_M'' = \chi_M' - 217$; in c.g.s. units. [b] $\mu_{eff}^T = 2{\cdot}84\sqrt{\chi_M''.T}$; in B.M.

TABLE 9

Magnetic susceptibility data for $Cr[N(SiMe_3)_2]_3$

T (K)	$(10^6\chi_M')$ [a]	(μ_{eff}^T) [b]
298 [c]	5843	3·74
273	6433	3·74
248	6953	3·72
223	7833	3·74
198	8913	3·76
173	9903	3·71
123	13,893	3·70

[a] Values in c.g.s. units; averaged from three field strengths. [b] In B.M.; with $\theta = -4°$. [c] A measurement in solution (methyl cyclohexane) gave $\chi_M' = 5863 \times 10^{-6}$ c.g.s.; $\mu_{eff} = 3{\cdot}74$.

TABLE 10

Magnetic susceptibility data for $Fe[N(SiMe_3)_2]_3$

T (K)	$(10^6\chi_M')$ [a]	(μ_{eff}^T) [b,c]
298	14,290	5·94
273	15,440	5·93
223	18,690	5·93
173	23,700	5·92
123	32,750	5·91
98	40,820	5·94

[a] Values in c.g.s. units; averaged from three field strengths and involve two independent experiments. [b] In B.M.; with $\theta = -10°$. [c] Using Evans' n.m.r. method with cyclohexane solvent gave $\chi_M' = 11{,}663 \times 10^{-3}$ c.g.s. at 310 K corresponding to $\mu_{eff} = 5{\cdot}4 \pm 0{\cdot}1$.

in vacuo. After admission of pure nitrogen the tube was capped with a B-5 standard ground-glass joint.

The values of χ_M obtained were independent of field strength and the average of the determinations at three fields was taken and corrected for diamagnetic contributions (Pascal's constants) to give χ_M'. The reciprocal $(\chi_M')^{-1}$ was plotted against temperature (K) to check that the compounds obeyed the Curie–Weiss law and θ was obtained by extrapolation from the least-squares best fit to a straight line. The magnetic moment $\mu_{eff}{}^T$ was evaluated from the expression $\mu_{eff}{}^T = 2{\cdot}84\ [\chi_M'(T - \theta)]^{\frac{1}{2}}$.

The results are given in Tables 8—10 for M[N(SiMe$_3$)$_2$] (M = Ti, Cr, and Fe). For M = V it was not possible to complete a variable-temperature experiment but from $\chi_M' = 2362 \times 10^{-6}$ c.g.s. at 298 K assuming Curie law behaviour gave $\mu_{eff} = 2{\cdot}38$.

We thank the S.R.C. for an award (E. C. A.) and for the e.s.r. equipment, the Royal Society for a reflectance attachment for the Beckmann DK-2A, and Queen Mary College for a studentship (R. G. C.).

[2/1512 *Received*, 28*th June*, 1972]

APPENDIX

The following tables give the electrostatic interaction matrices for the configurations d^2, d^3, and d^5 (partially) in D_{3h} symmetry in terms of the Racah parameters A, B, and C. The complete interaction matrices are obtained by adding the strong field contributions to the diagonal terms. All the matrices are symmetric.

TABLE A1

d^2 Matrices

	$^3A_2'$	$(e'')^2$	$(e')^2$
$^3A_2'$		$A - 5B$	$6B$
$(e'')^2$			$A + 4B$
$(e')^2$			

$^3A_1''$, $^3A_2''$; $e''e'$: $A - 8B$

	$^3E''$	$a_1'e''$	$e''e'$
$^3E''$		$A + B$	$3\sqrt{6}B$
$a_1'e''$			$A - 2B$
$e''e'$			

$^3E'$; $a_1'e'$: $A - 8B$

	$^1A_1'$	$(a_1')^2$	$(e'')^2$	$(e')^2$
$^1A_1'$		$A + 4B + 3C$	$\sqrt{2}(B + C)$	$\sqrt{2}(4B + C)$
$(a_1')^2$			$A + 7B + 4C$	$6B + 2C$
$(e'')^2$				$A + 4B + 4C$
$(e')^2$				

	$^1E''$	$a_1'e''$	$e''e'$
$^1E''$		$A + 3B + 2C$	$-\sqrt{6}B$
$a_1'e''$			$A - 2B + 2C$
$e''e'$			

	$^1E'$	$a_1'e'$	$(e'')^2$	$(e')^2$
$^1E'$		$A + 2C$	$2\sqrt{3}B$	0
$a_1'e'$			$A + B + 2C$	0
$(e'')^2$				$A + 4B + 2C$
$(e')^2$				

$^1A_1''$, $^1A_2''$; $e''e'$: $A + 4B + 2C$

TABLE A2

d^3 Matrices

	$^4A_2'$	$a_1'(e'')^2$	$a_1'(e')^2$
$^4A_2'$		$3A - 3B$	$-6B$
$a_1'(e'')^2$			$3A - 12B$
$a_1'(e')^2$			

$^4A_2''$, $^4A_1''$; $a_1'e''e'$: $3A - 15B$

	$^4E''$	$a_1'e''e'$	$e''(e')^2$
$^4E''$		$3A - 9B$	$-3\sqrt{6}B$
$a_1'e''e'$			$3A - 6B$
$e''(e')^2$			

$^4E'$; $(e'')^2e'$: $3A - 15B$

	$^2E''$	$(a_1')^2e''$	$(e'')^3$	$(a_1'e''e')_a$	$(a_1'e''e')_b$	$[e''(e')^2]_a$	$[e''(e')^2]_b$	$[e''(e')^2]_c$
$^2E''$		$3A + 7B + 4C$	$B + C$	$\sqrt{3}B$	$9B$	0	$\sqrt{2}(4B + C)$	0
$(a_1')^2e''$			$3A - 3B + 4C$	$\sqrt{3}B$	$3B$	$3\sqrt{6}B$	$\sqrt{2}(3B + C)$	0
$(e'')^3$				$3A - 6{\cdot}5B + 3C$	$(9/\sqrt{12})B$	$3\sqrt{2}B$	$2\sqrt{6}B$	0
$[a_1'e''e']_a$					$3A - 1{\cdot}5B + 3C$	0	$3\sqrt{2}B$	0
$[a_1'e''e']_b$						$3A + 3B + 3C$	$3\sqrt{3}B$	0
$[e''(e')^2]_a$							$3A - 3B + 5C$	0
$[e''(e')^2]_b$								$3A - 6B + 3C$
$[e''(e')^2]_c$								

	$^2E'$	$a_1'(e'')^2$	$(a_1')^2e'$	$[(e'')^2e']_a$	$[(e'')^2e']_b$	$[(e'')^2e']_c$	$a_1'(e')^2$	$(e')^3$
$^2E'$		$3A + 4B + 3C$	$-\sqrt{6}B$	$-3B$	$-5\sqrt{3}B$	0	0	0
$a_1'(e'')^2$			$3A - 8B + 4C$	0	$\sqrt{2}(B + C)$	0	0	$4B + C$
$(a_1')^2e'$				$3A - 6B + 3C$	$3\sqrt{3}B$	0	0	$3\sqrt{6}B$
$[(e'')^2e']_a$					$3A + 5C$	0	0	$\sqrt{2}(3B + C)$
$[(e'')^2e']_b$						$3A - 9B + 3C$	$-\sqrt{6}B$	0
$[(e'')^2e']_c$							$3A - 8B + 3C$	0
$a_1'(e')^2$								$3A + 12B + 4C$
$(e')^3$								

	$^2A_2'$	$a_1'(e'')^2$	$(e'')^2e'$	$a_1'(e')^2$
$^2A_2'$		$3A + 3C$	$3\sqrt{2}B$	$-6B$
$a_1'(e'')^2$			$3A - 3B + 3C$	$-3\sqrt{2}B$
$(e'')^2e'$				$3A + 3C$
$a_1'(e')^2$				

	$^2A_1'$	$a_1'(e'')^2$	$(e'')^2e'$	$a_1'(e')^2$
$^2A_1'$		$3A + 10B + 5C$	$-5\sqrt{6}B$	$6B + 2C$
$a_1'(e'')^2$			$3A - 3B + 3C$	$-\sqrt{6}B$
$(e'')^2e'$				$3A - 8B + 5C$
$a_1'(e')^2$				

	$^2A_1''$, $^2A_2''$	$(a_1'e''e')_a$	$(a_1'e''e')_b$	$e''(e')^2$
$(a_1'e''e')_a$		$3A - 0{\cdot}5B + 3C$	$(3\sqrt{3}/2)B$	$4\sqrt{3}B$
$(a_1'e''e')_b$			$3A - 7{\cdot}5B + 3C$	$6B$
$e''(e')^2$				$3A + 3C$

TABLE A3

d^5 Matrices (not the doublet states)

$^6A_1'$; $a_1'(e'')^2(e')^2$: $10A - 35B$

$^4E''$	$a_1'(e'')^3e'$	$(e'')^3(e')^2$	$(a_1')^2e''(e')^2$	$a_1'e''(e')^3$
$a_1'(e'')^3e'$	$10A - 19B + 6C$	$-2\sqrt{6}B$	$-\sqrt{6}B$	$-C$
$(e'')^3(e')^2$		$10A - 23B + 6C$	$B + C$	$\sqrt{6}B$
$(a_1')^2e''(e')^2$			$10A - 23B + 6C$	$2\sqrt{6}B$
$a_1'e''(e')^3$				$10A - 19B + 6C$

$^4E'$	$(a_1')^2(e'')^2e'$	$[a_1'(e'')^2(e')^2]_a$	$[a_1'(e'')^2(e')^2]_b$	$(e'')^2(e')^3$
$(a_1')^2(e'')^2e'$	$10A - 17B + 6C$	0	$-\sqrt{6}B$	$4B + C$
$[a_1'(e'')^2(e')^2]_a$		$10A - 25B + 5C$	0	0
$[a_1'(e'')^2(e')^2]_b$			$10A - 22B + 5C$	$\sqrt{6}B$
$(e'')^2(e')^3$				$10A - 17B + 6C$

$^4A_1''$, $^4A_2''$	$a_1'(e'')^3e'$	$a_1'e''(e')^3$
$a_1'(e'')^3e'$	$10A - 19B + 6C$	$6B + C$
$a_1'e''(e')^3$		$10A - 19B + 6C$

$^4A'_2$	$[a_1'(e'')^2(e')^2]_a$	$[a_1'(e'')^2(e')^2]_b$
$[a_1'(e'')^2(e')^2]_a$	$10A - 13B + 7C$	0
$[a_1'(e'')^2(e')^2]_b$		$10A - 28B + 7C$

$^4A_1'$	$[a_1'(e'')^2(e')^2]_a$	$[a_1'(e'')^2(e')^2]_b$
$[a_1'(e'')^2(e')^2]_a$	$10A - 25B + 5C$	0
$[a_1'(e'')^2(e')^2]_b$		$10A - 18B + 5C$